Published in final edited form as:

Clin Cancer Res. 2017 January 01; 23(1): 250–262. doi:10.1158/1078-0432.CCR-16-0081.

A Strong B-cell Response Is Part of the Immune Landscape in Human High-Grade Serous Ovarian Metastases

Anne Montfort[1], **Oliver Pearce**[1], **Eleni Maniati**[1], **Benjamin G. Vincent**[2], **Lisa Bixby**[2], **Steffen Böhm**[1,3], **Thomas Dowe**[1], **Edmund H. Wilkes**[1], **Probir Chakravarty**[4], **Richard Thompson**[1], **Joanne Topping**[1], **Pedro R. Cutillas**[1], **Michelle Lockley**[1,3], **Jonathan S. Serody**[2], **Melania Capasso**[1], and **Frances R. Balkwill**[1]

[1]Barts Cancer Institute, Queen Mary University of London, London, UK

[2]Line-berger Comprehensive Cancer Center, Inflammatory Diseases Institute, Departments of Medicine and Microbiology and Immunology, University of North Carolina, Chapel Hill, North Carolina

[3]Medical Oncology, Barts Health NHS Trust, London, UK

[4]Bioinformatics Core, The Francis Crick Institute, London, UK

Abstract

Purpose—In high-grade serous ovarian cancer (HGSOC), higher densities of both B cells and the $CD8^+$ T-cell infiltrate were associated with a better prognosis. However, the precise role of B cells in the antitumor response remains unknown. As peritoneal metastases are often responsible for relapse, our aim was to characterize the role of B cells in the antitumor immune response in HGSOC metastases.

Experimental Design—Unmatched pre and post-chemotherapy HGSOC metastases were studied. B-cell localization was assessed by immunostaining. Their cytokines and chemokines were measured by a multiplex assay, and their phenotype was assessed by flow cytometry. Further

Corresponding Authors: Frances R. Balkwill, Queen Mary University of London, Charterhouse Square, London EC1M 6BQ, UK. Phone: 207-882-3851; Fax: 207-882-3885; f.balkwill@qmul.ac.uk; and Melania Capasso, m.capasso@qmul.ac.uk.
M. Capasso and F.R. Balkwill contributed equally to this article.

Note: Supplementary data for this article are available at Clinical Cancer Research Online (http://clincancerres.aacrjournals.org/).

Disclosure of Potential Conflicts of Interest: No potential conflicts of interest were disclosed.

Authors' Contributions: Conception and design: A. Montfort, M. Capasso, F.R. Balkwill
Development of methodology: A. Montfort, B. Vincent
Acquisition of data (provided animals, acquired and managed patients, provided facilities, etc.): A. Montfort, O. Pearce, B. Vincent, L. Bixby, S. Böhm, T. Dowe, E.H. Wilkes, R. Thompson, J. Topping, P.R. Cutillas, M. Lockley
Analysis and interpretation of data (e.g., statistical analysis, biostatistics, computational analysis): A. Montfort, O. Pearce, E. Maniati, B. Vincent, E.H. Wilkes, P. Chakravarty, P.R. Cutillas, J.S. Serody
Writing, review, and/or revision of the manuscript: A. Montfort, E. Maniati, S. Böhm, T. Dowe, M. Lockley, J.S. Serody, M. Capasso, F.R. Balkwill
Administrative, technical, or material support (i.e., reporting or organizing data, constructing databases): A. Montfort, B. Vincent, S. Böhm, R. Thompson, J. Topping
Study supervision: A. Montfort, M. Capasso, F.R. Balkwill

in vitro and *in vivo* assays highlighted the role of B cells and plasma cell IgGs in the development of cytotoxic responses and dendritic cell activation.

Results—B cells mainly infiltrated lymphoid structures in the stroma of HGSOC metastases. There was a strong B-cell memory response directed at a restricted repertoire of antigens and production of tumor-specific IgGs by plasma cells. These responses were enhanced by chemotherapy. Interestingly, transcript levels of CD20 correlated with markers of immune cytolytic responses and immune complexes with tumor-derived IgGs stimulated the expression of the costimulatory molecule CD86 on antigen-presenting cells. A positive role for B cells in the antitumor response was also supported by B-cell depletion in a syngeneic mouse model of peritoneal metastasis.

Conclusions—Our data showed that B cells infiltrating HGSOC omental metastases support the development of an antitumor response.

Introduction

The immune system can both limit and promote cancer development. Immune cells infiltrate tumors, and recent trials showed how unleashing a tumor-specific immune response with the use of tumor vaccines or immune checkpoint blockade can constitute a successful cancer therapy (1, 2). The majority of cancer immunology studies have concentrated on the protumor or antitumor abilities of T cells or myeloid cells. Less is known about the role of B cells in the tumor micro-environment, especially their contribution to the metastatic niche. In preclinical models of melanoma, squamous cell carcinoma and carcinogen-induced skin cancer, B cells promote tumor progression through the production of immune regulatory cytokines and immune complexes (IC; refs. 3–5). On the other hand, in human primary tumors, the presence of B cells in association with tertiary lymphoid structures (TLS) in non-small cell lung carcinoma (NSCLC) and colorectal, ovarian, and pancreatic cancers has been associated with a better prognosis (6–9). In these tumors, the presence of both B cells and dendritic cells (DC) correlated with an increase in Th1 signature, which might explain the correlation with better survival.

Very few studies have described the immune landscape of human metastases. Lymphoid structures were identified in cutaneous metastases of melanoma patients (10) as well as in lung metastases of colorectal cancer and renal cell carcinoma (RCC) patients (11). Interestingly, a high infiltration of $CD8^+$T cells and DC-$LAMP^+$ DCs correlated with an increased overall survival (OS) of patients with colorectal cancer, whereas this correlated with decreased OS of patients with RCC (11). B cells have been described in TLS; however, their role in the tumor immune landscape remains unclear. In primary ovarian cancer biopsies, intratumor infiltration of $CD27^-$ atypical memory B cells, together with $CD8^+$ T cells, is linked to better prognosis (12). A very recent study also showed that a high infiltrate of T cells, B cells, and plasma cells in primary tumors is linked to the presence of TLS in the microenvironment and improved survival of patients (13). Whether B cells behave the same way in ovarian cancer metastases and how they influence the antitumor response is unknown.

The term ovarian cancer refers to a group of five diseases defined as high-grade serous, low-grade serous, mucinous, endometrial, and clear cell carcinomas that are known to arise from different organs and have different molecular and transcriptomic profiles but all spread into the peritoneal cavity (14, 15). High-grade serous ovarian cancer (HGSOC) is the most common subtype, representing about 70% of cases and the majority of deaths from ovarian cancer (14). Early detection of the disease is one of the biggest challenges, as most patients are diagnosed at an advanced stage with metastases disseminated in the peritoneal cavity. Platinum-based chemotherapy and surgical de-bulking represent the baseline treatment for HGSOC and can prolong survival, although the majority of patients eventually relapse and die of peritoneal disease. Therefore, understanding the biological properties of the peritoneal metastases and their immune infiltrate is essential to develop new treatment strategies that target the tumor deposits responsible for relapse.

In order to elucidate the role of B cells in omental metastasis from HGSOC patients, we analyzed 92 omental samples obtained after surgery. B cells were located mainly in lymphoid aggregates, which displayed characteristic features of TLS. The majority of B cells had a memory phenotype, displayed a restricted clonal repertoire compared with peripheral healthy B cells and produced cytokines and chemokines known to recruit and activate antitumor immune cells, such as DCs, T cells and NK cells. Using RNAseq analyses and *in vivo* experiments, we also showed that B cells are implicated in immune cytotoxic responses.

Furthermore, B cells differentiated to plasma cells and produced immunoglobulins (Ig) against tumor targets. Igs can be found bound to antigen-presenting cells (APC) in the tumor stroma, coculture of APCs with ICs generated *in vitro* with tumor IgGs increased the expression of the costimulatory molecule CD86, suggesting that Igs might promote an antitumor response through potentiation of DC priming. Overall, our data suggest that B cells favor the development of an antitumor immune response in omental metastasis of HGSOC.

Materials and Methods

Patient samples

Omental tissues were collected from HGSOC patients (FIGO stage III and IV) prior to or following platinum-based chemotherapy treatment (Supplementary Table S1). Samples were either formalin fixed and paraffin embedded or snap frozen and stored at − 80°C or processed as fresh tissues. Blood samples from pre-and post-chemotherapy patients were collected in sodium heparin tubes for plasma separation and EDTA tubes for cell analysis. Control blood was collected from 12 healthy volunteers. Institutional review board approval was granted for the Barts Gynae Tissue Bank to collect and store biological material and clinical information. Patients were treated at St Bartholomew's Cancer Centre between 2010 and 2016 and gave written informed consent. Clinical parameters were collected using tissue repository databases and chart review.

Cell lines

The AOCS1 cell line was kindly given by Professor David Bowtell (Peter MacCallum Cancer Centre, Melbourne, Australia) and was established from the ascites of a patient diagnosed with HGSOC, Silverberg Grade 3, after second relapse.The G33 cell line was established in our laboratory from an omental HGSOC tumor collected during interval debulking surgery in 2011 (16). The cell lines have been authenticated. Cells were cultured in DMEM/F12 (Gibco), 10% FCS, 2 mmol/L L-glutamine, 1% penicillin and streptomycin in a 5% CO2 humidified incubator at 37° C. Regular checks for mycoplasma contamination were performed.

Tissue processing and flow cytometry

The stroma vascular fraction (SVF) was isolated from fresh omentum by mechanical dissection of the tissue with a scalpel and collagenase D digestion for 30 minutes at 37°C (Roche). Digested samples were filtered through 70-μm strainers, and the SVF were used for FACS analyses. Fresh peripheral blood mono-nuclear cells (PBMC) were isolated from blood samples by centrifugation with Ficoll-Paque Plus (GE Healthcare).

Cell suspensions were stained with different antibody panels for 30 minutes on ice in PBS, 2.5% bovine serum albumin, and 2 mmol/L EDTA. Cells were then washed twice and analyzed directly by FACS or fixed in PBS 2% formalin for 10 minutes at 4°C before being analyzed. Antibodies and viability dyes are shown in Supplementary Table S2. Appropriate fluorescence minus one (FMO) controls were used in these experiments. Analysis was performed using an LSR Fortessa cell analyzer (BD Biosciences).

Immunostaining of FFPE sections

Paraffin-embedded sections from HGSOC omental metastases were stained for CD20, CD4, CD8, IgG, IgM, CD68, Ki67, FDC, Myeloperoxidase (MPO; Dako), MECA79 (Biolegend), and DC-LAMP (Sigma). Sections were deparaffinized in xylene for 10 minutes and re-hydrated by successive immersion in 100%, 90%, 70%, 50% EtOH and H_2O. Heat-induced antigen retrieval was performed with Citrate Buffer (Vector Labs) for 20 minutes in a pressure cooker.

Immunohistochemistry—Slides were blocked in PBS 2.5% BSA and 2.5% goat serum for 40 minutes at room temperature (RT) and biotin/streptavidin blocking buffer (Vector Labs) according to the manufacturer's recommendations. Primary and secondary antibodies were applied for 1 hour at RT. Enzymatic activity was revealed with the Vectastain ABC Elite kit (Standard; Vector Labs) and Sigma FAST 3,3-diaminobenzidine tablets (Sigma). Sections were counterstained with hematoxylin and mounted with DPX mounting medium (Sigma).

For dual-stain immunohistochemistry, antibodies were incubated sequentially and revealed with the Vectastain system previously described. FAST 3,3-diaminobenzidine tablets were used to generate the brown color, and the Immpact VIP peroxidase substrate kit (SK-4605 Vector labs) generated the purple color. Sections were mounted with Dako Faramount aqueous mounting medium.

Brightfield pictures we taken with an Axiophot microscope (Zeiss). CD20, DC-LAMP, and MPO single-stained slides were scanned using a Pannoramic Scanner (3D HISTECH) and analyzed with the “Tissue Studio” software 4.0 (Definiens).

To assess numbers of MPO^+ neutrophils and DC-$LAMP^+$ DCs in lymphoid structures, 2 to 5 TLS per tumor were analyzed to obtain a mean number of positive cells per TLS for each metastasis. Intravessel cells were excluded from the counts.

Immuno fluorescence—Slides were incubated for 20 minutes in NH_4 Cl (50 mmol/L) to reduce autofluorescence and blocked in PBS 2.5% BSA, 2.5% goat serum for 40 minutes at RT. IgG staining was performed prior to any other additional staining. Subsequently, primary antibodies were applied overnight at 4° C. The next day, fluorescently labeled secondary antibodies (Invitrogen) were incubated for 1 hour at RT, and sections were mounted with Prolong gold antifade reagent containing Dapi (Thermo Fisher Scientific).

The specificity of the stainings was determined using appropriate isotype controls. Fluorescent pictures were taken with an LSM510 confocal microscope (Zeiss).

In vitro DC differentiation and activation

PBMCs were isolated from the blood of 6 healthy volunteers by centrifugation with Ficoll-Paque Plus (GE Healthcare). $CD14^+$ monocytes were purified using anti-human CD14 beads (Miltenyi) and cultured in RPMI 10% FCS, 20 ng/mL recombinant human GM-CSF and recombinant human IL4 (Biolegend). After 6 days, monocyte-derived DCs were re-stimulated with 10 μg/mLof IgGs (purified from protein extracts of two HGSOC omental tumors or healthy plasma IgGs and pooled) for 24 hours, pre-incubated or not with 30 mg of combined protein extracts from HGSOC cell lines G33 and AOCS1. Expression of the costimulation marker CD86 on DCs was assessed by flow cytometry.

Statistical analysis

Data are expressed as the mean of values per sample ± SEM. Statistical significance for flow cytometry, immunohistochemistry, and Mesoscale analyses was assessed using the Student *t* test or a nonparametric test (Mann-Whitney) when appropriate. Spear-man or Pearson tests were used for correlation analyses. Data normal distribution was assessed using the D Agostino & Pearson omnibus normality test. Data were considered statistically significant from $P < 0.05$.

For the mouse experiment, luminescence intensity values were $\log_{10}$ transformed before applying a one-way ANOVA test to account for heteroscedasticity of results.

For BCR sequencing data analyses, we used the species richness, the Gini-Simpson index and the Shannon entropy as diversity indexes.

Finally, for the RNAseq data analysis, significantly differentially expressed genes were identified using a double threshold of false discovery rate (FDR) < 0.05 and an absolute fold change > 2.

Results

Presence of B cells in TLS in HGSOC omentum is associated with the generation of memory B-cell responses

To assess the presence and localization of B cells in HGSOC omental metastases, paraffin sections from unmatched biopsies taken pre- ($n = 10$) and post- ($n = 31$) neoadjuvant chemotherapy (NACT) were stained for the B-cell marker CD20 (Supplementary Table S3). $CD20^+$ B cells were localized mainly in lymphoid aggregates in the stroma, next to tumor islets (Fig. 1A and B). There was no significant difference in the number of B cells in pre and post NACT biopsies, suggesting that chemotherapy neither impairs nor increases B-cell infiltration in omental metastases (Fig. 1C). Because similar lymphoid structures were described in other solid cancers as TLS (7, 10, 17), we further characterized the B-cell-rich follicles using immunohistochemistry and immunofluorescence. We often observed a core of $CD20^+$ B cells surrounded by a T-cell-rich area of mainly $CD4^+$ T cells, whereas $CD8^+$ T cells were located at the periphery of the lymphoid aggregates (Fig. 1D). In addition, high endothelial venules (HEV; blood vessels specialized in the recruitment of immune cells within lymphoid organs) were present, as indicated by MECA79 staining (Fig. 1E). By double-color immunohistochemistry we also identified areas rich in follicular DCs and $Ki67^+$ highly proliferative germinal center B cells surrounded by $CD45RO^+$ memory cells (Fig. 1F). Taken together, these features indicate the presence of TLS in HGSOC omental metastases.

TLS are implicated in the differentiation of antigen-specific B cells and development of memory responses (8). To assess the B-cell composition of HGSOC omental metastases, flow cytometry analysis of cells extracted from 25 fresh HGSOC omenta was carried out. Results showed that a majority of omental B cells display a “classical” ($CD27^+IgM^+$ and $CD27^+IgM^-$) or “atypical” ($CD27^-IgM^-$) memory phenotype (Fig. 2A and B). Interestingly, we observed a significant increase in the proportion of class-switched memory B cells ($CD27^+IgM^-$) in metastases from NACT-treated patients compared with pre-chemotherapy patients (Supplementary Fig. S1A). This was accompanied by a decrease in $CD20^+$-naïve B cells after chemotherapy treatment, although data did not reach statistical significance. The extent of residual disease did not seem to impact significantly on the proportion of class-switched memory B cells after chemotherapy (Supplementary Fig. S1A).

The percentage of naïve B cells was on average 28.2% of $CD20^+$ cells in omental metastasis (Fig. 2B), lower than that in patient blood (mean 47.8%; Supplementary Fig. S1B). This difference suggested that there was an ongoing B-cell response in HGSOC patients that drove B-cell differentiation and might have taken place in TLS at sites of metastasis.

Further analyses of B-cell subpopulations demonstrated that a higher proportion of class-switched memory B cells ($CD20^+CD27^+IgM\sim$ and $CD20^+CD27^-IgM^-$) expressed the costimulatory molecule CD86 when compared with IgM^+ memory ($CD27^+IgM^+$) and naive ($CD27^-IgM^+$) B cells (Fig. 2C). No difference in CD86 expression was observed between pre and post chemotherapy patients (Supplementary Fig. S1C). Nonetheless, all memory B-cell subpopulations also upregulated the inhibitory receptor PD1, albeit to a lesser extent

(Fig. 2D; Supplementary Fig. S1D). Coexpression of CD86 and PD1 on B cells was generally low (Supplementary Fig. S1E and S1F).

To investigate whether omental B cells were mounting an antigen-specific response, we then analyzed their clonal repertoire by B-cell receptor (BCR) sequencing. We extracted RNA from purified omental HGSOC B cells and peripheral B cells from healthy individuals and sequenced the *IgH* portion of the B-cell receptor. We report here three common mathematical indices of diversity calculated from the *IgH* repertoire data: the species richness (defined as the number of unique *IgH* clono-types in the sample), the Shannon entropy (which equally weights a species richness term and a term that increases with increasing clonal dominance), and the Gini–Simpson index (which weights the dominance term more heavily than the species richness term). For all diversity indices, HGSOC B cells showed decreased diversity relative to healthy donor B cells (Fig. 2E). This observation was in accordance with an increase in the rate of somatic hypermutations in Igs from HGSOC omentum compared with healthy B cells (Fig. 2F).

So far, our results suggest that B cells in HGSOC omentum are activated, differentiate to a memory B-cell phenotype and undergo clonal selection.

B cells correlate with the infiltration of DC-LAMP$^+$ DCs and an immune cytolytic signature in HGSOC omentum

B cells secrete proinflammatory and/or regulatory cytokines and chemokines that can influence the development of specific immune responses, as previously found in different cancer models (18, 19). To determine how the secretome of HGSOC B cells could influence the antitumor immune response, B cells from omental metastases were purified and stimulated for 48 hours with a low dose of PMA and Ionomycin (PMA/Iono). The secretion of cytokines and chemokines was analyzed by electroche-moluminescence multiplex assay and healthy peripheral B cells were used as a control.

The heatmap shown in Fig. 3A highlights the relationship existing between 24 cytokines and chemokines produced by HGSOC omental B cells and suggests an immune-stimulatory role for B cells. In addition to secretion of cytokines and chemokines (GM-CSF, IFNγ, IL12p40, CXCL10, and IL7) that can broadly recruit and support macrophages, DCs, T cells, and NK cells, tumor omental B cells produced significant amounts of inflammatory cytokines, such as CXCL8, CCL2 and IL6, even in the absence of PMA/ionomycin stimulation (Fig. 3B-D). Median concentrations were 19,694 pg/mL for CXCL8, 885.5 pg/mL for CCL2, and 51.4 pg/mL for IL6, as opposed to 2,178 pg/mL, 2.19 pg/mL and 2.027 pg/mL, respectively, in HGSOC and healthy peripheral B cells.

When we analyzed the expression of the CXCL8 receptors CXCR1 and CXCR2 on immune cells from HGSOC omentum we observed that, in accordance with previously published evidence (20), granulocytes expressed the highest levels of both receptors, whereas DCs expressed significant but lower levels of CXCR1 and CXCR2 (Fig. 3E). B and T cells had very low expression of these two chemokine receptors. These results suggest that through the production of CXCL8, B cells are implicated in the recruitment of both DCs and granulocytes in omental metastases and more specifically in TLS. Given that the majority of

granulocytes in HGSOC omentum are neutrophils (data not shown), we stained HGSOC omental tumors for the neutrophil marker MPO (myeloperoxidase) and DC marker DC-LAMP and assessed the localization of DCs and neutrophils in the tumor microenvironment (Fig. 3F). Three times less neutrophils than DCs were observed in TLS. We next studied whether there was a correlation between the number of $CD20^+$ B cells and DC-$LAMP^+$ DCs in HGSOC omentum. Immunohistochemistry staining and digital analysis of 16 FFPE sections from HGSOC omental metastases showed a significant correlation between the density of B cells and DCs in the stroma area of omental tumors (Fig. 3G).

In lung cancer, thepresence of B-cell–rich TLS and DCs has been linked to good prognosis and the development of a Th1 signature (21). Because activated DCs can stimulate $CD8^+$ T cells and promote a cytotoxic response and B cells and DC densities were correlated in HGSOC metastases (Fig. 3G), we assessed whether the B-cell infiltrate correlated also with a cytotoxic response. To this end, we analyzed RNA from HGSOC omental metastasis by RNAseq and examined transcriptional changes between uninvolved stage 1/2 HGSOC omentum ($n = 6$), stage 3/4 untreated ($n = 4$), chemotherapy-treated diseased omentum (bad responders; $n = 7$), and chemotherapy-treated omentum with low residual disease (good responders; $n = 5$). When comparing gene expression levels between these groups, 44 genes, characteristic of a B-cell signature, were significantly increased in omental metastases (stage 3/4 pre and post chemo and stage 3/4 good responders as opposed to stage 1/2; Fig. 4A–D). We next analyzed the correlation between the transcript levels of *CD20* in stage 3/4 HGSOC omentum and the immune cytotoxic markers *granzyme A (GZMA)* and *perforin (PRF1*; ref. 22). Not only did we observe a strong correlation between the levels of *CD20* and *GZMA or PRF1* transcripts (Pearson r = 0.73 and 0.61, respectively; data not shown) but *CD20* expression also strongly correlated with the geometric mean of the combined parameters (Fig. 4E). This suggested that B cells contribute favorably to the development of an antitumor immune response.

The above associations were supported by an experiment using a syngeneic mouse model of ovarian cancer, in which the mouse cell line ID8 is injected intraperitoneally and tumor growth is monitored over the course of 8 weeks. We depleted $CD20^+$ B cells in tumor-bearing mice with an anti-CD20 antibody and found that B-cell depletion was associated with an increased tumor progression (Fig. 4F, left) and a reduced T-cell cytotoxic activity, as indicated by decreased expression of the degranulation marker CD107 from asciticCD8$^+$T cells (Fig. 4F, bottom right).

Collectively, our results suggest that through the production of cytokines and chemokines that help recruit and support antigen-presenting cells, B cells could enhance the development of an immune cytotoxic response toward tumor cells.

Immunoglobulin production by intratumor plasma cells

Active germinal center reactions in TLS are normally associated with differentiation of plasma cells that secrete antigen-specific immunoglobulins. Indeed, HGSOC omenta appeared to contain a plasma cell infiltrate, as demonstrated by the presence of $CD38^{++}CD19^{+/-}$ $CD20^-CD27^+$ cells (Fig. 5A and B). Furthermore, we observed high levels of IgG deposits in HGSOC omenta, mainly located in stromal areas but also bound to tumor

cells and macrophages (Fig. 5C). IgM immunoglobulins were also detected but to a lesser extent (Supplementary Fig. S2A). Mass spectrometry analysis of proteins extracted from three HGSOC omental metastases confirmed that IgG immunoglobulins represent the largest subclass, with IgM and IgA representing less than 15% of total antibodies. IgE immunoglobulins were not detected under these conditions (Supplementary Fig. S2B).Wenext examined the amount of IgG1, IgG2, IgG3, and IgG4 subclasses in HGSOC omenta from different disease stages (1/2 vs. 3/4) with high or low residual disease (Supplementary Table S4). Figure 5D shows an increase in the presence of IgG1, IgG2, and IgG3 in stage 3/4 omenta compared with stages 1/2 (Fig. 5D; Supplementary Fig. S2C). Furthermore, IgG3 was significantly increased in post-chemotherapy diseased samples compared with pretreatment samples. On the other hand, IgG4 levels seemed to increase in stage 3/4 prechemotherapy tumors compared with stage 1/2 uninvolved omenta but had a tendency to decrease post-chemotherapy. Importantly, HGSOC patient plasma levels of IgG sub-classes were not different from healthy controls (Supplementary Table S5 and Supplementary Fig. S2D and S2E), suggesting that a tumor-specific antibody response preferentially takes place at the tumor site in TLS.

Next, to assess the ability of omental IgGs to recognize membrane bound and/or intracellular tumor antigens, we isolated immunoglobulins from three HGSOC omental tumors (G146, G168, and G175) and tested their reactivity toward intact or permeabilized tumor cells (AOCS1 and G33 HGSOC cell lines) by flow cytometry and immunofluorescence, respectively (Supplementary Fig. S3A–S3C). IgGs from all three omenta mainly targeted intracellular antigens, either cytoplasmic or nuclear (Supplementary Fig. S3A and B); nonetheless, IgGs extracted from the G175 and G146 omental tumors were able to recognize antigens expressed at the surface of a subpopulation of the HGSOC tumor cell line AOCS1 (Supplementary Fig. S3C).

To determine the nature of these antigens, we carried out immunoprecipitation experiments using purified tumor immunoglobulins as bait and assessed proteins pulled down by mass spectrometry. Total tumor lysate and control bead extracts were used as controls. Proteins found enriched in the IP fraction (but not in the control bead extracts) compared with the total tumor lysate were considered potential targets of intratumor IgGs (Table 1).This assay identified a number of targets of omental IgGs,some of which were validated by IHC. The proteins GNA13 (Guanine nucleotide binding protein (G) 13),DPYSL3 (Dihydropyrimidase like 3 or CRMP4), and HSPB1 (heat shock protein B1) were detected in paraffin sections of HGSOC omenta (Supplementary Fig. S3D).We concluded from these experiments that the majority of immunoglobulins were binding antigens released inthe tumor microenvironment after tumor cell death. Nevertheless, the extensive deposition of immunoglobulins bound to antigens, called immune complexes (ICs), could still be playing a role in the antitumor response, because ICs can activate APCs via ligation of Fc gamma receptors (FcγR; refs. 23, 24). Therefore, we assessed whether purified intratumor IgGs were playing a role in the activation of APCs *in vitro*. In these experiments, we treated monocyte-derived DCs with tumor-derived IgGs, preincubated or not with protein extracts from HGSOC cell lines in order to generate ICs. IgGs from healthy blood, alone or incubated with tumor antigens, were used as controls (Fig. 5E). Treatment of monocyte-derived DCs with *in vitro*–generated tumor ICs significantly increased the expression of the costimulatory molecule CD86

compared with healthy IgGs in combination with tumor antigens. This suggested that IgGs, likely produced by intratumor plasma cells, recognize tumor antigens and form ICs that contribute to the activation of APCs in the tumor microenvironment.

Discussion

In this study, we set out to elucidate the role played by B cells in HGSOC metastases by analyzing human biopsies. From previous studies, it was known that high levels of $CD8^+$ T-cell infiltration of primary human ovarian tumors were associated with an increased survival (25) and that patients displaying high tumor-infiltrating T cells, $CD20^+$ B cells and plasma cells exhibited an additional survival advantage (12, 13). This was reinforced by analyses of the TCGA ovarian cancer dataset, showing a positive correlation between a B-cell gene expression signature and progression-free survival in immunoreactive ovarian tumors (26). However, data were limited to primary tumors and not peritoneal metastases, which are generally responsible for the high rate of recurrence in HGSOC. In our work on omental metastases, we found that B cells in HGSOC omentum were mainly located in lymphoid structures and a high proportion exhibited a memory pheno-type. These results were in accordance with those of the above-mentioned study demonstrating memory B cells in primary ovarian tumors, which correlated with a good prognosis (12). Furthermore, a similar role for B cells was also described in NSCLC (8). We do not have sufficient samples to assess correlations with survival; nonetheless, our results indicate that B cells take part and positively influence the development of an antitumor response. This is in agreement with a preclinical study showing that depletion of B cells using anti-CD20 antibodies in the B16 melanoma model impairs $CD8^+$ T-cell antitumor immunity and promotes cancer development (27). Interestingly, we observed that depletion of B cells in the ID8 ovarian mouse model decreased the expression of the degranulation marker, CD107, on $CD8^+$ T cells. This was accompanied by increased tumor growth and suggested that depletion of B cells impairs the T-cell–dependent antitumor cytotoxic response. In accordance with these results, RNAseq analyses of human omental metastases showed CD20 transcript levels significantly correlated with levels of cytolytic markers (22), hence linking B cells to immune cytotoxic responses in patients' metastases.

It is interesting to note that chemotherapy neither affected the enrichment in B-cell signature nor the density of $CD20^+$ B cells; however, class-switched memory B cells were enhanced after NACT. Although we cannot rule out a direct effect of chemotherapy on survival and migration of B cells, it is possible to speculate that following chemotherapy the release of tumor antigens in the microenvironment provides a boost for the activation and differentiation of B cells. Nonetheless, these results are in accordance with studies describing the immune-stimulatory properties of chemotherapeutic agents such as anthracyclins, which causes immunogenic cell death of tumor cells (28) and platinum-based chemotherapy, shown to promote T-cell activation and down-regulation of immune-modulatory molecules on DCs (29). Our results indicate that chemotherapy has a positive influence also on B-cell responses.

Next, we observed that omental B cells produced a network of cytokines and chemokines, including IFNγ, IL12, GM-CSF and CXCL10, compatible with the development of

antitumor responses, most likely occurring within TLS. HGSOC omental B cells also secreted high amounts of CXCL8, a chemoattractant for neutrophils and DCs. Indeed, CXCR1 and CXCR2 receptors for CXCL8 were detected on omental DCs and neutrophils. Although neutrophils expressed higher levels of both receptors, more DCs than neutrophils infiltrated the lymphoid structures found in omental metastases. A more complex chemotactic network comprising CCL2, CXCL8, GM-CSF but also additional unidentified factors might explain this observation. Interestingly and in accordance with a study conducted in NSCLC (8), stromal densities of $CD20^+$ B cells and DC-$LAMP^+$ DCs correlated in omental tumors. *In vitro* studies recently demonstrated that activated B cells could induce the maturation of monocyte-derived DCs, rendering them competent for T-cell activation (30). Whether omental B cells directly support maturation of DCs in a similar fashion remains to be determined. None-theless, the spatial distribution of B cells and DCs within the TLS and B-cell cytokine and chemokine production suggest that B cells promote not only DC recruitment but also their differentiation. Are B cells also involved in increasing DC antigen-presenting ability? In this respect, we observed a high deposition of IgGs in the tumor stroma, some of which were bound to APCs. Several factors might contribute to this stromal localization: (i) the extracellular matrix could impair the diffusion of IgGs, preventing them from reaching tumor cells; (ii) ongoing cell death due to necrosis, chemotherapy, and/or immunity, which favors the release of antigens in the microenvironment, hence sequestering antigen-specific IgGs in the stroma; (iii) IgGs targeting intracellular antigens that cannot be easily accessible. We confirmed that intratumor IgGs preferentially target intracellular antigens, although some cytoplasmic proteins can be abnormally exposed at the surface of cancer cells (31). Nonetheless, previous studies provided evidence that Igs targeting intracellular antigens possess anticancer properties either by reaching their targets, possibly through internalization by cancer cells (32, 33) or by activating APCs through FcR, which in turn stimulate T-cell responses (34). In support of this latest hypothesis, we found that immunoglo-bulins from HGSOC metastases can form ICs with tumor antigens and promote expression of the coactivatory molecule CD86 on *in vitro* generated DCs. These results indicate that ICs present in the tumor stroma could increase DC antigen-presenting capabilities.

Contrary to studies showing an increase in IgG4 antibodies in cutaneous metastases of melanoma patients (35), the pre-dominance of IgG1, IgG2, and IgG3 over IgG4 antibodies in HGSOC metastases, especially following chemotherapy treatment, highlighted their potential to trigger APC activation, through binding to activatory FcgRs (36, 37). It is interesting to note that in post-chemotherapy omentum displaying low residual disease, the decrease in tumor IgGs, mirrored by the decrease in the B-cell infiltrate in the tumor, is likely to be linked to a partial resolution of the antitumor immune response with a decreased number of TLS.

In conclusion, our study demonstrated for the first time that in human metastases of HGSOC, B cells develop memory responses in the tumor microenvironment, likely via their association with TLS. In this context, their activated phenotype, secretion of proimmunogenic cytokine/chemokines and production of IgGs targeting tumor antigens is associated with an enhanced recruitment and priming of DCs and promotion of immune cytotoxic responses. Our study provides supporting evidence that ICs of antitumor IgGs

bound to tumor antigens could be beneficial in the clinic and potentiate antitumor responses. This approach has already been tested in a preclinical study (23) and should be further explored in a cancer setting. Because we show that chemotherapy further enhances the antitumor B-cell response, these new approaches would be compatible and aided by current treatments.

Supplementary Material

Refer to Web version on PubMed Central for supplementary material.

Acknowledgments

We wish to thank the patients and healthy donors for consenting to donate samples as well as the surgeons of Barts Health NHS, Ms. Elly Brockbank, Mr. Arjun Jeyarajah, Mr. Ranjit Manchanda, Ms. AlexandraLawrence, and Mr. David Oram. We also thank Barts Health NHS Trust pathologists Dr. Naveena Singh and Dr. Asma Faruqi. We also wish to thank George Elia and Dr. Linda Hammond, Barts Cancer Institute, for their technical supportaswellas Professor David Bowtell, Darius Etemadmoghadam, and Chris Mitchell (MacCallum Cancer Center, Melbourne, Australia) for providing the AOCS1 cell line. Finally, we would like to thank Genentech for providing us with the anti-CD20 antibody used in our *in vivo* experiment.

Grant Support: This work was funded by Cancer Research UK (A16354), Swiss Cancer League (BIL KLS2883-02-2012), the European Research Council (ERC322566), Barts and The London Charity (467/1307 to M. Lockley and BLT 297/2249 to P.R. Cutillas), Bloodwise (Bennett Fellowship to M. Capasso, ref 12002), UNC University Cancer Research Fund and UNC Oncology Clinical Translational Research Training Program (5K12CA120780, to B. Vincent), and NCI (P50 CA058223, to J.S. Serody).

References

1. Bloy N, Pol J, Aranda F, Eggermont A, Cremer I, Fridman WH, et al. Trial watch: dendritic cell-based anticancer therapy. Oncoimmunology. 2014; 3:e963424. [PubMed: 25941593]
2. Homicsko K, Coukos G. Targeting programmed cell death 1 in ovarian cancer. J Clin Oncol. 2015; 33:3987–9. [PubMed: 26503205]
3. de Visser KE, Korets LV, Coussens LM. De novo carcinogenesis promoted by chronic inflammation is B lymphocyte dependent. Cancer Cell. 2005; 7:411–23. [PubMed: 15894262]
4. Schioppa T, Moore R, Thompson RG, Rosser EC, Kulbe H, Nedospasov S, et al. B regulatory cells and the tumor-promoting actions of TNF-alpha during squamous carcinogenesis. Proc Natl Acad Sci U S A. 2011; 108:10662–7. [PubMed: 21670304]
5. Ammirante M, Luo JL, Grivennikov S, Nedospasov S, Karin M. B-cell-derived lymphotoxin promotes castration-resistant prostate cancer. Nature. 2010; 464:302–5. [PubMed: 20220849]
6. Dieu-Nosjean MC, Antoine M, Danel C, Heudes D, Wislez M, Poulot V, et al. Long-term survival for patients with non-small-cell lung cancer with intratumoral lymphoid structures. J Clin Oncol. 2008; 26:4410–7. [PubMed: 18802153]
7. Bindea G, Mlecnik B, Tosolini M, Kirilovsky A, Waldner M, Obenauf AC, et al. Spatiotemporal dynamics of intratumoral immune cells reveal the immune landscape in human cancer. Immunity. 2013; 39:782–95. [PubMed: 24138885]
8. Germain C, Gnjatic S, Tamzalit F, Knockaert S, Remark R, Goc J, et al. Presence of B cells in tertiary lymphoid structures is associated with a protective immunity in patients with lung cancer. Am J Respir Crit Care Med. 2014; 189:832–44. [PubMed: 24484236]
9. Hiraoka N, Ino Y, Yamazaki-Itoh R, Kanai Y, Kosuge T, Shimada K. Intratumoral tertiary lymphoid organ is a favourable prognosticator in patients with pancreatic cancer. Br J Cancer. 2015; 112:1782–90. [PubMed: 25942397]
10. Cipponi A, Mercier M, Seremet T, Baurain JF, Theate I, van den Oord J, et al. Neogenesis of lymphoid structures and antibody responses occur in human melanoma metastases. Cancer Res. 2012; 72:3997–4007. [PubMed: 22850419]

11. Remark R, Alifano M, Cremer I, Lupo A, Dieu-Nosjean MC, Riquet M, et al. Characteristics and clinical impacts of the immune environments in colorectal and renal cell carcinoma lung metastases: influence of tumor origin. Clin Cancer Res. 2013; 19:4079–91. [PubMed: 23785047]
12. Nielsen JS, Sahota RA, Milne K, Kost SE, Nesslinger NJ, Watson PH, et al. CD20^{+}tumor-infiltrating lymphocytes have an atypical CD27-memory phenotype and together with CD8+Tcells promote favorable prognosis in ovarian cancer. Clin Cancer Res. 2012; 18:3281–92. [PubMed: 22553348]
13. Kroeger DR, Milne K, Nelson BH. Tumor-infiltrating plasma cells are associated with tertiary lymphoid structures, cytolytic T-cell responses, and superior prognosis in ovarian cancer. Clin Cancer Res. 2016; 22:3005–15. [PubMed: 26763251]
14. Bowtell DD, Bohm S, Ahmed AA, Aspuria PJ, Bast RC Jr, Beral V, et al. Rethinking ovarian cancer II: reducing mortality from high-grade serous ovarian cancer. Nat Rev Cancer. 2015; 15:668–79. [PubMed: 26493647]
15. Vaughan S, Coward JI, Bast RC Jr, Berchuck A, Berek JS, Brenton JD, et al. Rethinking ovarian cancer: recommendations for improving outcomes. Nat Rev Cancer. 2011; 11:719–25. [PubMed: 21941283]
16. Milagre CS, Gopinathan G, Everitt G, Thompson RG, Kulbe H, Zhong H, et al. Adaptive upregulation of EGFR limits attenuation of tumor growth by neutralizing IL6 antibodies, with implications for combined therapy in ovarian cancer. Cancer Res. 2015; 75:1255–64. [PubMed: 25670170]
17. Goc J, Fridman WH, Sautes-Fridman C, Dieu-Nosjean MC. Characteristics of tertiary lymphoid structures in primary cancers. Oncoimmunology. 2013; 2:e26836. [PubMed: 24498556]
18. Balkwill F, Montfort A, Capasso M. B regulatory cells in cancer. Trends Immunol. 2013; 34:169–73. [PubMed: 23206438]
19. Nelson BH. CD20+ B cells: the other tumor-infiltrating lymphocytes. J Immunol. 2010; 185:4977–82. [PubMed: 20962266]
20. Grob PM, David E, Warren TC, DeLeon RP, Farina PR, Homon CA. Characterization of a receptor for human monocyte-derived neutrophil chemotactic factor/interleukin-8. J Biol Chem. 1990; 265:8311–6. [PubMed: 2186041]
21. Goc J, Germain C, Vo-Bourgais TK, Lupo A, Klein C, Knockaert S, et al. Dendritic cells in tumor-associated tertiary lymphoid structures signal a Th1 cytotoxic immune contexture and license the positive prognostic value of infiltrating CD8^{+} T cells. Cancer Res. 2014; 74:705–15. [PubMed: 24366885]
22. Rooney MS, Shukla SA, Wu CJ, Getz G, Hacohen N. Molecular and genetic properties of tumors associated with local immune cytolytic activity. Cell. 2015; 160:48–61. [PubMed: 25594174]
23. Schuurhuis DH, Ioan-Facsinay A, Nagelkerken B, van Schip JJ, Sedlik C, Melief CJ, et al. Antigen–antibody immune complexes empower dendritic cells to efficiently prime specific CD8^{+} CTL responses in vivo. J Immunol. 2002; 168:2240–6. [PubMed: 11859111]
24. Regnault A, Lankar D, Lacabanne V, Rodriguez A, Thery C, Rescigno M, et al. Fcgamma receptor-mediated induction of dendritic cell maturation and major histocompatibility complex class I–restricted antigen presentation after immune complex internalization. J Exp Med. 1999; 189:371–80. [PubMed: 9892619]
25. Adams SF, Levine DA, Cadungog MG, Hammond R, Facciabene A, Olvera N, et al. Intraepithelial T cells and tumor proliferation: impact on the benefit from surgical cytoreduction in advanced serous ovarian cancer. Cancer. 2009; 115:2891–902. [PubMed: 19472394]
26. Iglesia MD, Vincent BG, Parker JS, Hoadley KA, Carey LA, Perou CM, et al. Prognostic B-cell signatures using mRNA-seq in patients with subtype-specific breast and ovarian cancer. Clin Cancer Res. 2014; 20:3818–29. [PubMed: 24916698]
27. DiLillo DJ, Yanaba K, Tedder TF. B cells are required for optimal CD4^{+} and CD8^{+} T cell tumor immunity: therapeutic B cell depletion enhances B16 melanoma growth in mice. J Immunol. 2010; 184:4006–16. [PubMed: 20194720]
28. Casares N, Pequignot MO, Tesniere A, Ghiringhelli F, Roux S, Chaput N, et al. Caspase-dependent immunogenicity of doxorubicin-induced tumor cell death. J Exp Med. 2005; 202:1691–701. [PubMed: 16365148]

29. Lesterhuis WJ, Punt CJ, Hato SV, Eleveld-Trancikova D, Jansen BJ, Nierkens S, et al. Platinum-based drugs disrupt STAT6-mediated suppression of immune responses against cancer in humans and mice. J Clin Invest. 2011; 121:3100–8. [PubMed: 21765211]

30. Maddur MS, Sharma M, Hegde P, Stephen-Victor E, Pulendran B, Kaveri SV, et al. Human B cells induce dendritic cell maturation and favour Th2 polarization by inducing OX-40 ligand. Nat Commun. 2014; 5:4092. [PubMed: 24910129]

31. Weidle UH, Maisel D, Klostermann S, Schiller C, Weiss EH. Intracellular proteins displayed on the surface of tumor cells as targets for therapeutic intervention with antibody-related agents. Cancer Genomics Proteomics. 2011; 8:49–63. [PubMed: 21471515]

32. Guo K, Li J, Tang JP, Tan CP, Hong CW, Al-Aidaroos AQ, et al. Targeting intracellular oncoproteins with antibody therapy or vaccination. Sci Transl Med. 2011; 3:99ra85.

33. Hong CW, Zeng Q. Tapping the treasure of intracellular oncotargets with immunotherapy. FEBS Lett. 2014; 588:350–5. [PubMed: 24184114]

34. Noguchi T, Kato T, Wang L, Maeda Y, Ikeda H, Sato E, et al. Intracellular tumor-associated antigens represent effective targets for passive immunotherapy. Cancer Res. 2012; 72:1672–82. [PubMed: 22318866]

35. Karagiannis P, Gilbert AE, Josephs DH, Ali N, Dodev T, Saul L, et al. IgG4 subclass antibodies impair antitumor immunity in melanoma. J Clin Invest. 2013; 123:1457–74. [PubMed: 23454746]

36. Kalergis AM, Ravetch JV. Inducing tumor immunity through the selective engagement of activating Fcgamma receptors on dendritic cells. J Exp Med. 2002; 195:1653–9. [PubMed: 12070293]

37. Bruhns P, Iannascoli B, England P, Mancardi DA, Fernandez N, Jorieux S, et al. Specificity and affinity of human Fcgamma receptors and their polymorphic variants for human IgG subclasses. Blood. 2009; 113:3716–25. [PubMed: 19018092]

38. Venturi V, Kedzierska K, Turner SJ, Doherty PC, Davenport MP. Methods for comparing the diversity of samples of the T cell receptor repertoire. J Immunol Methods. 2007; 321:182–95. [PubMed: 17337271]

Translational Relevance

Little is known about how B cells interact with other players of the tumor immune landscape in HGSOC, especially in the context of a metastatic disease. The present study provides evidence for a positive role of B cells in the development of an antitumor immune response at metastatic sites, an effect that can be enhanced by chemotherapy treatment. A better understanding of these processes is essential for developing new anticancer immunotherapy strategies. We show that it would be beneficial to take advantage of B cells and their immunoglobulins to boost the antitumor immune responseinpatients with advanced-stage HGSOC, in particular to increase DC recruitment to tertiary lymphoid structures and their anti-gen-presenting ability. This could be exploited in dendritic cell–based vaccination protocols or as adjuvant to different anticancer treatments.

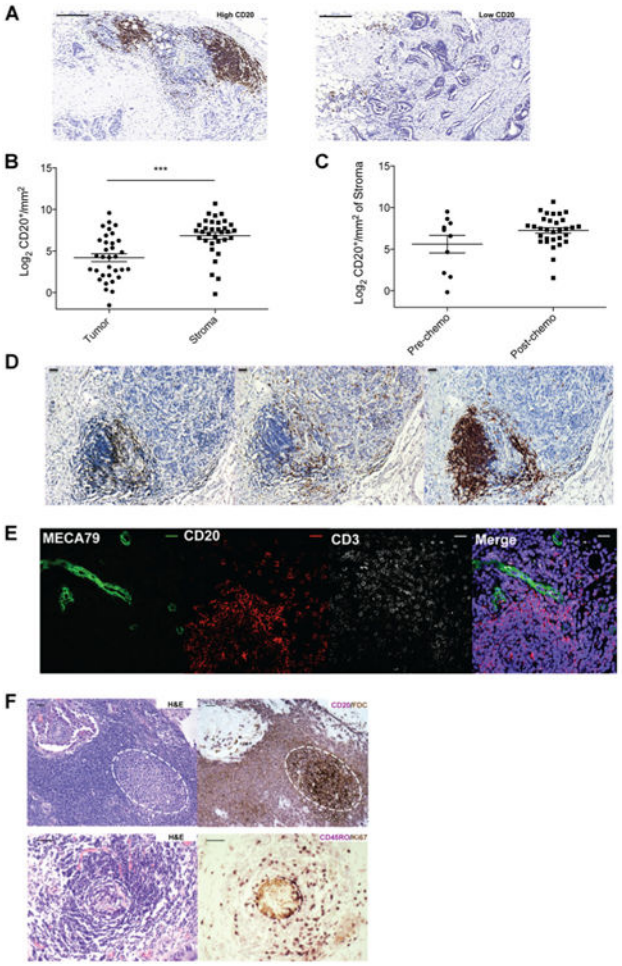

Figure 1.

B cells in HGSOC are found in tertiary lymphoid structures. **A**, Immunohistochemistry pictures showing two representative sections from paraffin-embedded HGSOC omentum stained for CD20. Scale bar, 200 μm. **B** and **C**, Log_2 density of $CD20^+$B cells in HGSOC omental metastases. **B**, Comparison of $CD20^+$ B cell densities in tumor versus stromal areas ($n = 33$; ***, $P < 0.001$; Mann-Whitney test). **C**, Comparison of $CD20^+$ B-cell densities in the stroma of unmatched HGSOC metastases obtained before ($n = 10$) and after chemotherapy treatment ($n = 31$). **D-F**, Characterization of the B-cell-rich lymphoid structures by single-color immunohistochemistry, immunofluorescence, and double-color immunohistochemistry. **D**, Identification of $CD20^+$ B cells, $CD4^+$, and $CD8^+$ T cells within TLS. Scale bars, 50 μm. **E**, Presence of MECA79+ high endothelial venules in TLS. Scale bars, 20 mm. F, Germinal centers of TLS contain follicular DCs (FDC) and $Ki67^+$ high proliferating cells surrounded by $CD45RO^+$ memory cells. Scale bars, 50 μm.

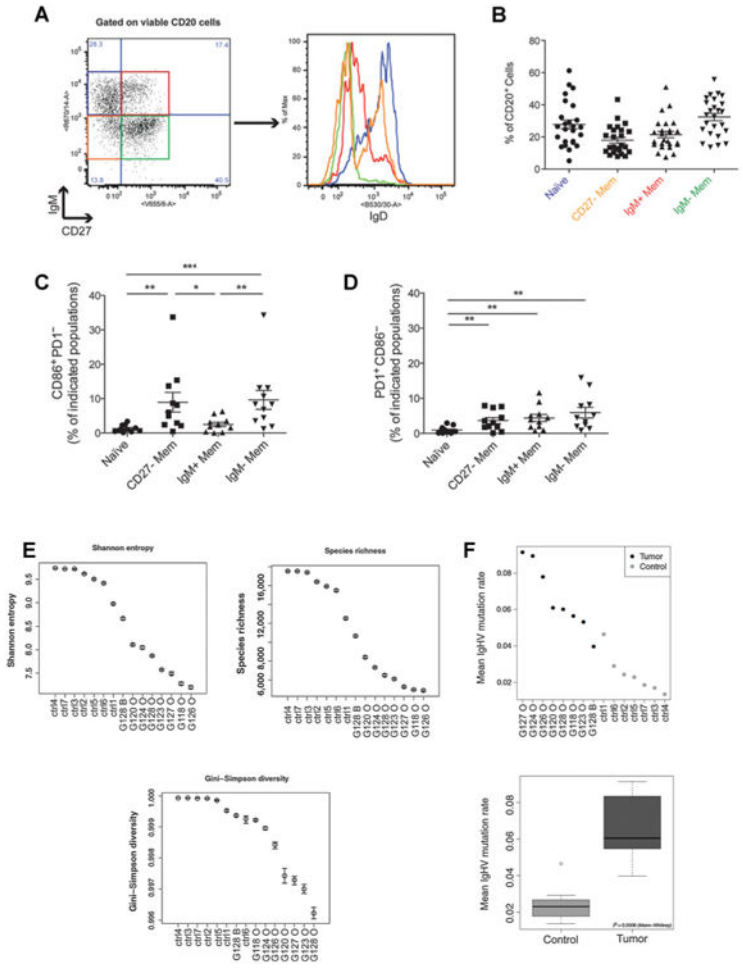

Figure 2.

Memory B-cell response in HGSOC metastases. **A** and **B**, Flow cytometry analysis of the B subpopulations in HGSOC omentum ($n = 25$) showing differential expression of CD27 and IgM within the $CD20^+$ cells. Representative plots (**A**) and percentages (**B**) of the different B-cell subpopulations: IgM^+ memory ($CD27^+IgM^+$), class-switched memory or IgM^- memory ($CD27^+IgM^-$), $CD27^-$ atypical memory ($CD27^-IgM^-$) and naive ($CD27^-IgM^+$) B cells. An example of IgD expression in the different subpopulations is shown. **C** and **D**, Proportion of $CD86^+PD1^-$ (**C**) and $PD1^+CD86^-$ (**D**) cells among the B-cell subsets described above ($n = 11$; *, $P < 0.05$; **, $P < 0.01$; ***, $P < 0.001$; Mann-Whitney test and Student t test). **E** and **F**, *BCR* sequencing of B cells from HGSOC omentum (O; $n = 7$) and blood (B; $n = 1$) compared with healthy peripheral B cells (ctrl; $n = 7$). **E**, Diversity analysis of the B-cell repertoire. Error bars, 95% confidence interval (38). **F**, Analysis of hypersomatic mutations. *IgH* mutation rates for each sample (top). Tumor and nontumor samples were binned and *IgHV* mutation rates were compared (bottom).

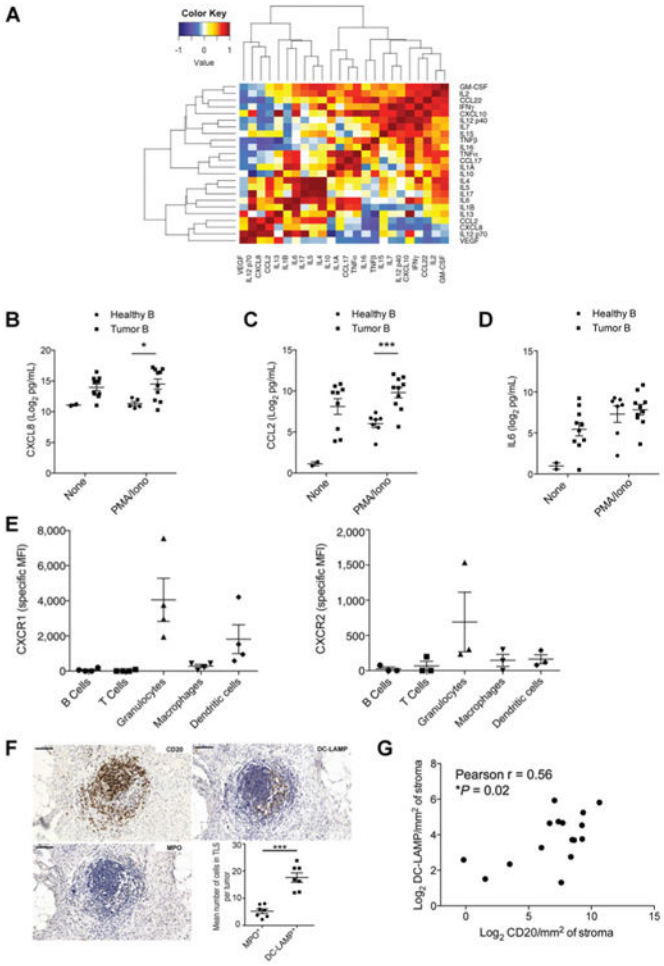

Figure 3.

Role of B cells in the recruitment of DCs in HGSOC metastases. **A**-**D**, Cytokine/chemokine secretion of HGSOC omental B cells (see Supplementary Methods). **A**, Correlation heatmap showing how the levels of the 24 cytokines and chemokines measured in the supernatant of HGSOC B cells ($n = 4–10$) vary with each other. Columns and rows represent individual cytokines and chemokines colored to indicate Pearson's correlation coefficient (r). **B**-**D**, Log_2 concentrations of CXCL8, CCL2, and IL6 in the supernatant of unstimulated healthy peripheral B cells ($n = 2$); PMA/ionomycin- (PMA/Iono) treated healthy peripheral B cells ($n = 5–7$); unstimulated and PMA/ionomycin-treated HGSOC omental B cells ($n = 9–10$; *, $P < 0.05$; ***, $P < 0.001$, Student t test). **E**, Flow cytometry analysis of CXCR1 ($n = 4$) and CXCR2 ($n = 3$) expression on $CD19^+$ B cells; $CD3^+$ T cells, $CD11b^{++}CD14^+CD11c^-$ macrophages; $CD11b^{++}CD14^-CD11c^-$ granulocytes and $CD11b^{++}$ $CD14^-CD11c^+$ DCs from HGSOC omentum. **F**, Representative immunostainings and quantification of DC-$LAMP^+$ DCs and MPO^+ neutrophils in $CD20^+$-rich lymphoid structures in HGSOC omental metastases ($n = 7$). Arrows indicate MPO^+ cells. Scale bar, 100 μm; ***, $P < 0.001$, Student t test. **G**, Correlation analysis between the log_2 densities of DC-$LAMP^+$ DCs and $CD20^+$ B cells in a cohort of 16 HGSOC patients (2 pre-chemotherapy and 14 post-chemotherapy; $P < 0.05$; Pearson correlation test).

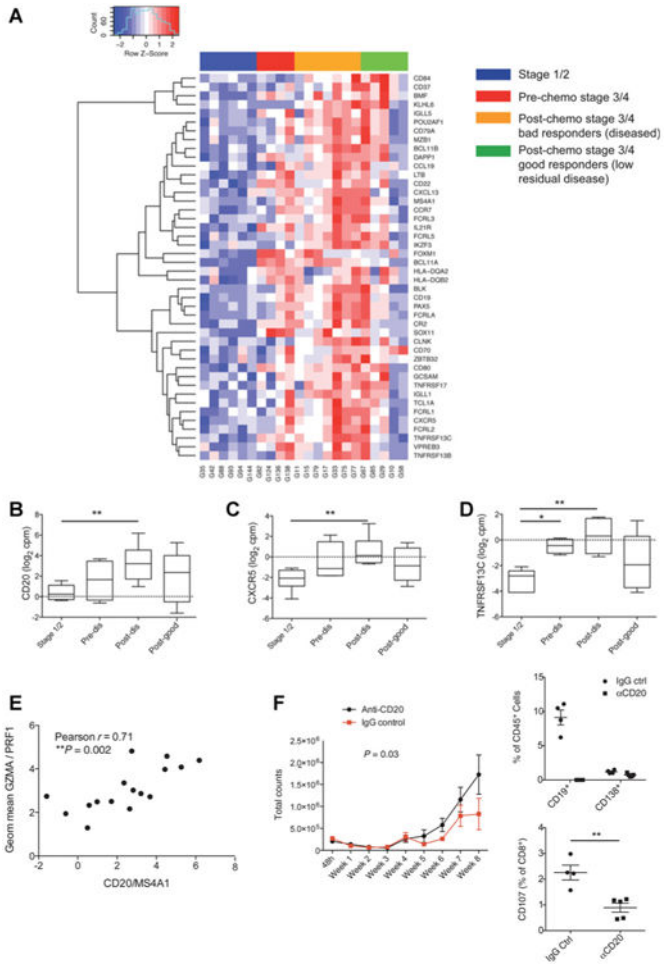

Figure 4.

B-cell signature is enriched in diseased omentum and linked to cytotoxic response. **A-D**, Heatmap and boxplots showing an increase in expression of B-cell signature genes in stage3/4 pre- ($n = 4$) and post-chemotherapy [post-chemotherapy diseased (post dis),$n = 7$; post-chemotherapy good responders (post good),$n = 5$)] vs. stage 1/2 ($n = 6$) non-involved HGSOC omentum. *, $P < 0.05$; **, $P < 0.01$; Student *t* test. **E**, Positive correlation between the geometrical mean of levels of expression of *granzymeA (GZMA)* and *perforin (PRF1)* versus *CD20 (MS4A1)* in HGSOC stage 3/4 omentum. **F**, CD20 depletion increased tumor progression in the ID8 mouse model. Left, tumor progression in anti-CD20- ($n = 5$) and IgG control- ($n = 4$) treated mice assessed by luciferase activity monitoring ($P = 0.03$; Two-way ANOVA on $\log_{10}$ luminescence values). Top right, Bcells ($CD45^+$ $CD19^+$) and plasma cells ($CD45^+$ $CD138^+$) are depleted in the ascitic fluid of αCD20-treated ID8 mice vs. IgG controls. Bottom right, CD107 expression by ascitic $CD8^+$ T cells in αCD20 and IgG control-treated ID8 mice (**, $P < 0.001$; Student *t* test).

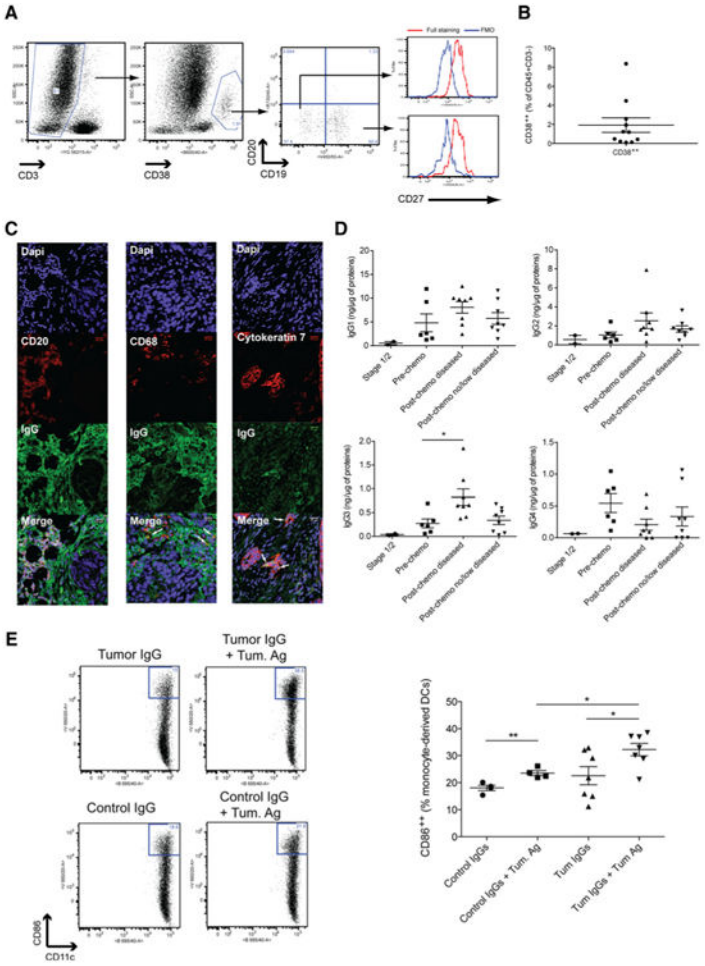

Figure 5.

Plasma cells are present in HGSOC omenta and IgGs deposited mainly in stromal areas but also on tumor cells and macrophages. **A** and **B**, Presence of $CD38^{+}$ $^{+}CD19^{+/-}CD20_CD27^{+}$plasma cells in HGSOC omentum (n =14; 11). **C**, Paraffin sections of omental metastases were fluorescently stained for CD20, CD68, or Cytokeratin 7 (CK7) (red) in combination with IgG (green). Arrows indicate colocalization of the CD68 and CK7 markers with IgG. Scale bar, 20 μm. **D**, Protein extracts isolated from frozen stage 3/4 pre-chemotherapy, post-chemotherapy diseased, post-chemotherapy with no/low residual disease and stage 1/2 noninvolved omentum were tested for the presence of human IgG1, IgG2, IgG3, and IgG4 by ELISA; * $P < 0.05$, Mann–Whitney. **E**, Tumor-derived IgGs ICs increase the expression of CD86 on DCs in vitro. IgGs were isolated from two tumor lysates using Agarose beads coupled to protein A/G and pooled. Monocyte-derived DCs (n =14; 7) from healthy volunteers were then treated with tumor IgGs alone or tumor IgGs preincubated with protein extracts from HGSOC tumor cells. IgGs from healthy plasma were used as a control. CD86 expression on DCs was assessed after 24-hour treatment.

Table 1

Proteins recognized by immunoglobulins in HGSOC omentum identified by mass spectrometry

				Enrichment compared with total extract		
	IgG targets	**Unique peptides, *n***	**Mascot *t* score**	**G175**	**G168**	**G146**
Pulled down from both G168 and G175 omentum	Guanine nucleotide-binding protein subunit alpha-13 OS=Homo sapiens GN=GNA13 PE=1 SV=2	1.0	92.8	1750.9	550.3	
	Protein 4.1 OS=Homo sapiens GN=EPB41 PE=1 SV=4	2.0	92.6	14.7	2.8	
Pulled down from G175 omentum only	Nexilin OS=Homo sapiens GN=NEXN PE=1 SV=1	3.0	78.3	177.4		
	60S acidic ribosomal protein P0 OS=Homo sapiens GN=RPLP0 PE=1 SV=1	3.0	188.8	11.7		
	Myosin light chain 6B OS=Homo sapiens GN=MYL6B PE=1 SV=1	3.0	146.1	25.2		
	CD5 antigen-like OS=Homo sapiens GN=CD5L PE=1 SV=1	1.0	83.7	26.6		
	Dihydropyrimidinase-related protein 2 OS=Homo sapiens GN=DPYSL2 PE=1 SV=1	4.0	180.5	2.6		
	60S ribosomal protein L6 OS=Homo sapiens GN=RPL6 PE=1 SV=3	4.0	153.6	3.8		
	Actin, aortic smooth muscle OS=Homo sapiens GN=ACTA2 PE=1 SV=1	2.0	962.8	5.6		
	Cell surface glycoprotein MUC18 OS=Homo sapiens GN=MCAM PE=1 SV=2	2.0	79.2	3.3		
	78 kDa glucose-regulated protein OS=Homo sapiens GN=HSPA5 PE=1 SV=2	8.0	370.0	2.7		
	Filamin-C OS=Homo sapiens GN=FLNC PE=1 SV=3	3.0	164.4	7.6		
	Dihydropyrimidinase-related protein 3 OS=Homo sapiens GN=DPYSL3 PE=1 SV=1	5.0	321.9	15.9		
	Inter-alpha-trypsin inhibitor heavy chain H1 OS=Homo sapiens GN=ITIH1 PE=1 SV=3	2.0	130.2	3.2		
	Interferon-induced GTP-binding protein Mx2 OS=Homo sapiens GN=MX2 PE=1 SV=1	2.0	218.2	64.0		
	Inter-alpha-trypsin inhibitor heavy chain H4 OS=Homo sapiens GN=ITIH4 PE=1 SV=4	4.0	164.4	4.2		
	AP-2 complex subunit alpha-1 OS=Homo sapiens GN=AP2A1 PE=1 SV=3	2.0	186.0	2.9		
	Keratin, type II cytoskeletal 8 OS=Homo sapiens GN=KRT8 PE=1 SV=7	1.0	137.5	2.7		
	40S ribosomal protein S20 OS=Homo sapiens GN=RPS20 PE=1 SV=1	2.0	103.9	3.2		
	Tripeptidyl-peptidase 1 OS=Homo sapiens GN=TPP1 PE=1 SV=2	1.0	83.1	4.4		
	Calreticulin OS=Homo sapiens GN=CALR PE=1 SV=1	2.0	90.6	8.9		
Pulled down from G168 omentum only	Hemoglobin subunit gamma-1 OS=Homo sapiens GN=HBG1 PE=1 SV=2	5.0	370.3		7.2	

Clin Cancer Res. Author manuscript; available in PMC 2018 May 01.

	IgG targets	Unique peptides, *n*	Mascot *t* score	Enrichment compared with total extract		
				G175	G168	G146
	Heat shock protein beta-1 OS=Homo sapiens GN=HSPB1 PE=1 SV=2	5.0	115.5		5.0	
	Histidine-rich glycoprotein OS=Homo sapiens GN=HRG PE=1 SV=1	2.0	101.9		3.6	
	Alpha-actinin-2 OS=Homo sapiens GN=ACTN2 PE=1 SV=1	1.0	470.3		2.6	
Pulled down from G146 omentum only	Desmin OS=Homo sapiens GN=DES PE=1 SV=3	1.0	101.8			31.8
	POTE ankyrin domain family member E OS=Homo sapiens GN=POTEE PE=1 SV=3	1.0	330.3			514.6

Note: Tumor IgGs were used as bait to immunoprecipitate their potential targeting antigens. Proteins found significantly enriched in the IP fractions compared with total tumor lysate were considered potential targets of tumor IgGs.